We are IntechOpen, the world's leading publisher of Open Access books Built by scientists, for scientists

4,800
Open access books available

122,000
International authors and editors

135M
Downloads

Our authors are among the

154
Countries delivered to

TOP 1%
most cited scientists

12.2%
Contributors from top 500 universities

CLARIVATE ANALYTICS BOOK CITATION INDEX INDEXED

WEB OF SCIENCE™

Selection of our books indexed in the Book Citation Index in Web of Science™ Core Collection (BKCI)

Interested in publishing with us?
Contact book.department@intechopen.com

Numbers displayed above are based on latest data collected.
For more information visit www.intechopen.com

26

Design of Optimum Weighting Functions for LFM Signals

Anatoliy Kononov, Lars Ulander and Leif Eriksson
Department of Radio and Space Science
Chalmers University of Technology, Gothenburg
Sweden

1. Introduction

Linear frequency-modulated (LFM) pulse signals are probably the most common type of pulse compression waveforms for various radar systems (Barton, 2005; Cook&Bernfeld, 1967; Curlander & McDonough, 1991; Levanon & Mozeson, 2004; Richards, 2005; Skolnik, 2008). LFM signals are also often the waveform of choice for wideband systems, where the required bandwidth may be hundreds of megahertz. The ambiguity function of the LFM signal suffers from significant sidelobes, both in delay (range) and in Doppler. It is known, for example, that the first range sidelobe is approximately 13 dB below the main peak of the ambiguity function. Such sidelobes may be unacceptable in many applications due to system performance degradation caused by high sidelobes (Cook & Bernfeld, 1967; Levanon & Mozeson, 2004; Richards, 2005). To suppress the sidelobes some form of weighting can be applied to the matched filter response. The main drawbacks associated with conventional weighting functions (e.g., Hamming, Kaiser windows) are the broadening of the main lobe of the ambiguity function cut along the time axis and an inevitable attenuation in the peak response which decreases the signal-to-noise ratio.

The chapter provides theoretical justification for a new approach, which is being applied to the design of discrete weighting function, or in other words, digital mismatched receiving filters. This approach considers the design of weighting functions as a problem of finding such a digital mismatched filter that will maximize the proportion of the total response power that is concentrated in the specified time-frequency region.

Two applications of the proposed approach are theoretically addressed in sections 2 and 3. First, in section 2, we apply it to the problem of the optimum Doppler-tolerant pair signal-filter design when a given signal is specified to be an LFM signal. Section 3 addresses the specification of weighting functions in interferometric synthetic aperture radars with the purpose of improving the height measurement accuracy. Both of these sections are supplimented with numerical results, which demonstrate benefits that one can derive from using the proposed optimum weigthing functions as compared to conventional weighting functions. Conclusions are given in section 4.

2. Design of Doppler-tolerant weighting functions

In this section we develop a method for designing weighting functions or, in other words, mismatched filters for LFM signals in order to minimize the sidelobe level at the filter

Source: Convergence and Hybrid Information Technologies, Book edited by: Marius Crisan,
ISBN 978-953-307-068-1, pp. 426, March 2010, INTECH, Croatia, downloaded from SCIYO.COM

output with respect to that of the LFM ambiguity function and preserve its Doppler-tolerant behaviour as much as possible. First, we review the Doppler tolerance of LFM signals in terms of their analog and digital ambiguity functions, then we briefly discuss the concept of digital cross-ambiguity function and then proceed to the design of the optimum Doppler-tolerant weighting functions and numerical examples.

2.1 Doppler tolerance of LFM signals

The complex envelope $u(t)$ of a linear frequency modulated pulse (LFM pulse or signal) of duration T , bandwidth B and unity energy is given by

$$u(t) = \frac{1}{\sqrt{T}} \exp(j\pi\alpha t^2), \ \alpha = \pm\frac{B}{T} \tag{2-1}$$

where α is the frequency slope. The time - bandwidth product of the LFM signal is simply defined as BT. Hence, for the LFM pulse to be qualified as a pulse compression waveform, this product has to meet the condition $BT >> 1$.

The ambiguity function $\chi(\tau, \nu)$ of an LFM pulse can be analytically presented as

$$\chi(\tau, \nu) = \left| \left(1 - \frac{|\tau|}{T}\right) \frac{\sin\left[\pi T(\nu + \alpha\tau)\left(1 - |\tau|/T\right)\right]}{\left[\pi T(\nu + \alpha\tau)\left(1 - |\tau|/T\right)\right]} \right|, \quad |\tau| < T; \quad \text{zero otherwise} \tag{2-2}$$

where τ is the shift in time and ν is the Doppler shift of the received signal relative to the nominal values expected by the matched filter. From (2-2), the peak of this sinc-like function occurs when $\nu + \alpha\tau = 0$, i.e., at points lying on the straight line $\tau = \mp \nu T/B$. All the peaks occur along this line represent a so-called skewed "ridge" of the ambiguity function of LFM signals. Hence, when $\nu = \nu_s \neq 0$, which means that there is a Doppler mismatch between an LFM signal received from a moving point target and corresponding matched filter, the peak of (2-2) will not occur at $\tau = 0$ as it takes place when there is no Doppler mismatch ($\nu = 0$). Instead, the peak will be shifted with respect to the point $\tau = 0$ by an amount τ_s that is proportional to the Doppler shift ν_s

$$\tau = \mp \nu T / B \tag{2-3}$$

This phenomenon is termed "range-Doppler" coupling. An estimate of the target range is based on the position of this peak in time. Hence, any non-zero Doppler shift ν_s of an LFM signal results in a range measurement error proportional to the shift in time specified by equation (2-3). As also follows from (2-2), taking into account (2-3), the amplitude of the peak will be reduced by the factor

$$\delta = 1 - |\tau_s| / T = 1 - |\nu_s| / B \, . \tag{2-4}$$

Fig. 2-1 sketches out the ridge-like behaviour of the LFM ambiguity function along the straight line $\tau = -\nu T/B$ and the relationships (2-3) and (2-4).

Let the reduction factor δ be bounded below by a value of b; it is clear that $0 \leq b \leq \delta \leq 1$. Using (2-4) yields the corresponding inequality for the acceptable Doppler shift

$$|\nu_s| \leq B\left(1 - 10^{0.05b}\right) \tag{2-5}$$

and, from equation $|\nu_s| = 2|V_t|/\lambda$, for the radial target velocity V_t

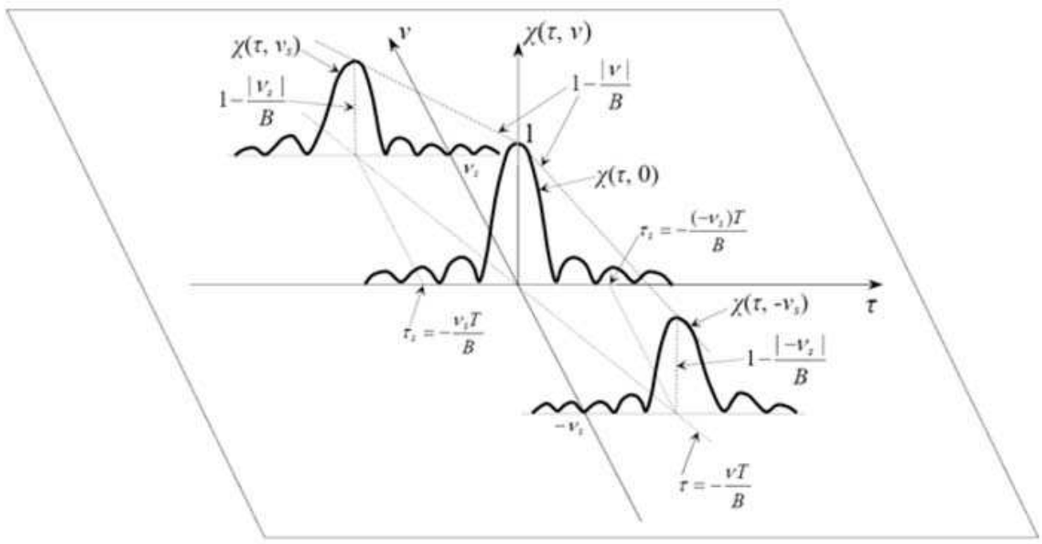

Fig. 2-1. Illusration of the ridge-like behaviour of the LFM ambiguity function

$$|V_t| \le 0.5\lambda B\left(1-10^{0.05b}\right) \tag{2-6}$$

where λ is the wavelength of the transmitted signal and b is specified in decibels.
Assuming B = 5 MHz, λ = 0.03m, and b = −0.1dB (this corresponds to b=0.9886≤δ ≤ 1) and using (2-5) and (2-6) yields $|\nu_s| / B \le 0.0114$ and $|V_t| \le 3090$ km/h, respectively. Hence, even for such a wide range of radial target velocity the reduction in amplitude at the output of the LFM matched filter does not exceed 0.1 dB (relative to the output peak for a zero-Doppler shift). Thus, one can conclude that Doppler tolerance is an intrinsic feature of the LFM signal, which reveals itself through the ridge of the LFM ambiguity function.
Athough the skewed ridge associated with the LFM ambiguity function causes errors in range and/or Doppler measurements it should be noted that the Doppler–tolerance of LFM signals can be an advantage in some applications. An example is in a search application since a preffered waveform to be used for target search should be Doppler-tolerant, so large Doppler shifts of targets whose velocity is not known does not prevent their detection due to a weak peak of the response at the matched filter output. This is also beneficial in terms of simplifying signal processor and detection hardware. If one were to use a biphase-coded signal in the same application one would need to have a bank of signal processors matched to a range of expected target Doppler shifts. This is because of the biphase-coded signal "thumbtack" ambiguity function, which features a single narrow central peak concentrated at the point $\tau = \nu = 0$, with the remaining energy spread uniformly all over the (τ, ν) plane (Levanon & Mozeson, 2004; Richards, 2005). Such features are useful for systems intended for high-resolution measurements in range and Doppler, or radar imaging.
Fig.2-2 compares the contours for the LFM ambiguity function and the ambiguity function of a biphase-coded signal. These contours correspond to a 3.92 dB level (Barton, 2005; Peebles, 1998) below maximum at (τ = 0, ν = 0). Both of the signals have equal pulse duration of T=MT_0 and bandwidth of $B \approx 1/T_0$, where M is the number of subpulses for the biphase-coded signal and T_0 is the duration of each subpulse.

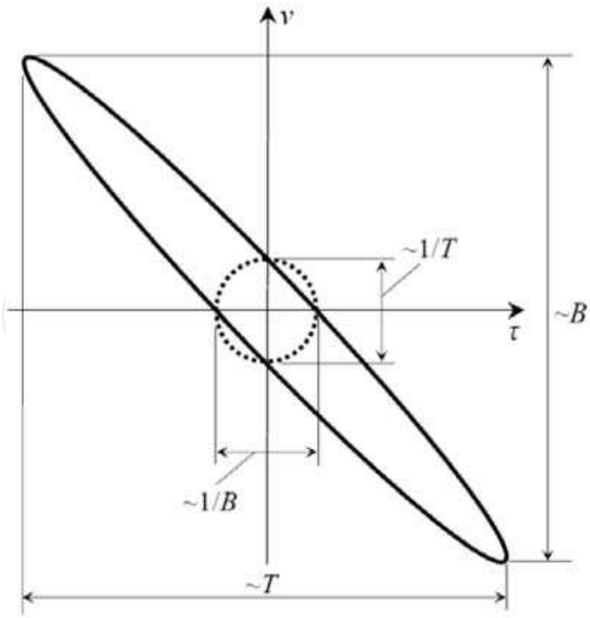

Fig. 2-2. Comparison of contours of ambiguity functions for LFM signal (solid line ellipse) and biphase-coded signal (dotted line circle) having the same pulse duration and badwidth

A disadvantage of the LFM ambiguity function is that it suffers from significant sidelobes, both in delay (range) and in Doppler. Consider, for example, a zero-Doppler cut of (2-2) $\chi(\tau\ ,\ 0)$, which is just the LFM matched filter output when there is no Doppler mismatch. Analyzing $\chi(\tau\ ,\ 0)$ under the condition $BT >> 1$, yelds that it exhibits the distinctly sinc-like main lobe and first few sidelobes (in magnitude). Due to this the first (and highest) range sidelobe in $\chi(\tau\ ,\ 0)$ is approximately equal to –13 dB and this value does not depend on the time-bandwidth product BT . Such a high sidelobe level is unacceptable in many applications since it may cause appreciable system performance degradation (Cook & Bernfeld, 1967; Levanon & Mozeson, 2004; Richards, 2005; Rosen et al., 2000).

2.2 Digital ambiguity function

The discussion in section 2.1 deals with analog LFM ambiguity function, i.e. it assumes that the LFM signal in radar receiver is processed by an ideal analog matched filter. Modern radar systems employ digital technologies so that it is instructive to discuss the features of a digital LFM ambiguity function that characterizes the response of a radar receiver when matched filtering is implemented by a digital signal processor.

First, we introduce a general relationship between the analog ambiguity function (analog matched filtering) and digital ambiguity function (digital implementation of the matched filter). In case of a point target the complex envelope of the received signal is given (ignoring amplitude coefficient) by $u(t-\tau)\exp[-j2\pi\nu(t-\tau)]$ where τ is the time delay and ν is the Doppler shift. Then, the complex envelope of a signal at the output of the analog filter matched to the transmitted signal $u(t)$ can be written as

$$\begin{aligned} A(t',\tau,\nu) &= \int_{-\infty}^{\infty} u(t-\tau)\exp[-j2\pi\nu(t-\tau)]\cdot u^*[-(t'-t)]dt \\ &= \exp[-j2\pi\nu(t'-\tau)]\cdot\int_{-\infty}^{\infty} u(t+t'-\tau)u^*(t)\mathrm{e}^{-j2\pi\nu t}\,dt. \end{aligned} \tag{2-7}$$

Expression (2-7) is usually simplified by dropping the insignificant phase factor $\exp[-j2\pi\nu(t'-\tau)]$ and replacing $t'-\tau$ with τ . Thus, we arrive at the definition of the complex ambiguity function

$$A_a(\tau,\nu)=\int_{-\infty}^{\infty}u(t+\tau)u^*(t)\mathrm{e}^{-j2\pi\nu t}\,dt \tag{2-8}$$

where subscript a stands for "analog". The analog ambiguity function is defined as the magnitude of (2-8)

$$\chi_a(\tau,\nu)=|A_a(\tau,\nu)|. \tag{2-9}$$

In digital receivers, the sampled complex envelope of the received signal can be represented as $u(nT_s-\tau)\exp[-j2\pi\nu(nT_s-\tau)]$, where n = ...,− 2,−1, 0, 1, 2, ..., and T_s is the sampling period that can be presented as $T_s=1/(gB)$, where $g\geq 1$ is the oversampling factor.
Since the unit sample response of the digital version of the matched filter is given by $u^*(-nT_s)$ the complex digital ambiguity function can be easily shown to be

$$A_d(\tau,\nu)=\sum_{n=-\infty}^{\infty}u(nT_s+\tau)u^*(nT_s)\mathrm{e}^{-j2\pi\nu nT_s}. \tag{2-10}$$

The definition for the digital ambiguity function is similar to (2-9)

$$\chi_d(\tau,\nu)=|A_d(\tau,\nu)|. \tag{2-11}$$

As has been shown (Blankenship & Hofstetter, 1975), there exists a simple relationship between the analog and digital ambiguity functions, which is given by

$$A_d(\tau,\nu)=\sum_{n=-\infty}^{\infty}A_a\left(\tau,\nu+nF_s\right) \tag{2-12}$$

where $F_s=1/T_s$ is the sampling frequency. Thus, the complex digital ambiguity function is a sum of the replicas of the complex analog ambiguity function displaced to all frequencies nF_s. Inspecting (2-12) yields that it is similar to the well known relationship between the Fourier transforms of an analog signal and its sampled version. It is also clear that equation (2-12) allows to quickly draw contour plots (ambiguity diagrams) for the digital LFM ambiguity functions at different sampling frequencies by using contour plots for the analog LFM anbuguity finction. The contour plots provide insight into the gross behavior of the LFM digital ambiguity function. Thus, for the purpose of detailed analysis an exact mathematical expresson for this function is necessary. As has been shown (Blankenship & Hofstetter, 1975), the exact formula for the digital LFM ambiguity function is given by

$$\chi_d(\tau,\nu)=\left|\frac{\sin\left[\pi\frac{N}{M}\left(k+x-\frac{M}{N}y\right)\left(1-\frac{|k|}{M}\right)\right]}{\sin\left[\pi\frac{N}{M^2}\left(k+x-\frac{M}{N}y\right)\right]}\right|,\ |k|\leq M-1 \tag{2-13}$$

Where $N=BT$, $y=vT$, and $M=T/T_s$ is the integer number of the LFM signal samples taken over the total signal duration T. Formula (2-13) assumes $\tau=(k+x)T_s$, where k is an integer and $0\leq x<1$.

Blankenship and Hofstetter studied the digital LFM ambiguity function by using (2-13) and contour plots. In particular, they have shown that in the digital case even with Nyquist rate sampling, i.e. with $T_s = 1/B$, the sidelobes do not fall off uniformly with increasing $|\tau|$, but increase as $|\tau|$nears the ends of the response interval ($\pm T$). The reason for this is that the aliased replicas of the analog ambiguity function produce increased sidelobe levels for large values of $|\tau|$. Hence, increasing the sampling rate should reduce this effect. Indeed, it has been shown that for sampling at twice the Nyquist rate, i.e., with $T_s = 1/(2B)$, the behavior of the digital LFM ambiguity functions is essentially indistinguishable from that of analog one. Here we supplement that study by illustrating the ridge (peak signal amplitude) for the digital LFM ambiguity function (Fig. 2-3) computed for $T_s = 1/B$ and $T_s = 1/(2B)$. Fig. 2-3 clearly demonstrates appreciable improvement in the Doppler tolerance for sampling at twice the Nyquist rate.

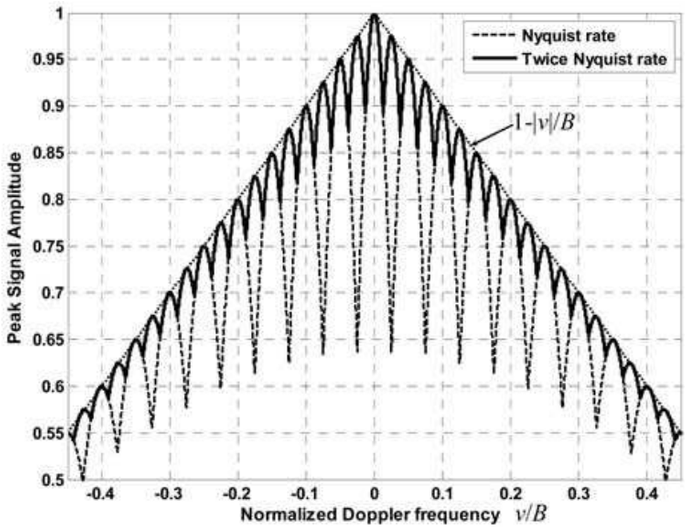

Fig. 2-3. Ridge (peak signal amplitude) of digital LFM ambiguity function versus Doppler frequency for different sampling rates; LFM signal parameters: B = 20 MHz, $T = 10^{-6}$ s

2.3 Digital cross-ambiguity function

This section introduces the concept of digital cross-ambiguity function that is directly related to digital signal processing based on mismatched filtering, which is more general structure than that based on the matched filter.

By analogy with (2-10) we have for the complex digital cross-ambiguity function

$$A_d^w(\tau,\nu) = \sum_{n=-\infty}^{\infty} u(nT_s+\tau)w^*(nT_s)\,\mathrm{e}^{-j2\pi\nu nT_s} \tag{2-14}$$

where $w^*(nT_s)$ corresponds to the unit sample response of the digital mismatched filter.

By letting $\tau = (k+x)T_s$, where k is an integer and $0 \le x < 1$, one can represent the samples of the received signal $u(nT_s+\tau)e^{-j2\pi\nu nT_s}$ in (2-14) as the column vector

$$u^x(\nu) = [u_1^x(\nu)\ u_2^x(\nu)\ \ldots\ u_N^x(\nu)]^{\mathrm{T}} \tag{2-15}$$

where $u^x(\nu) = [u_1^x(\nu)\ u_2^x(\nu)\ \ldots\ u_N^x(\nu)]^{\mathrm{T}}$. The integer k is omitted since in computing the output of a digital filter the time shift kT_s is a shift of the train of N received samples [vector

$u^x(v)$] by k samples [to the left if $k < 0$ or to the right if $k \geq 0$ when we look at the filtering operation as a complex correlator] with respect to N samples of the reference sequence specified by the vector $u^0(0)$.
Next, define a receiving filter vector w of length $M \geq N$

$$w = [w_1 \;\; w_2 \;\; \ldots \;\; w_M]^{\mathrm{T}} \tag{2-16}$$

Since the filter length M can be equal to or greater than N we will use the extended signal vector $s^x(v) = [s_1^x(v)\; s_2^x(v) \ldots s_M^x(v)]^{\mathrm{T}}$, which is zero-padded vector $u^x(v)$, to match the length M of the vector w . We define this extended signal vector as

$$s^x(v) = \begin{cases} [\underbrace{0\;0\;\ldots\;0}_{\text{(M-N)/2 zeros}}\; u_1^x(v)\; u_2^x(v) \ldots\; u_N^x(v)\; \underbrace{0\;0\;\ldots\;0}_{\text{(M-N)/2 zeros}}]^{\mathrm{T}}, & \text{if } M-N \text{ is even} \\ [\underbrace{0\;0\;\ldots\;0}_{\text{(M-N-1)/2 zeros}}\; u_1^x(v)\; u_2^x(v) \ldots\; u_N^x(v)\; \underbrace{0\;0\;\ldots\;0}_{\text{(M-N+1)/2 zeros}}]^{\mathrm{T}}, & \text{if } M-N \text{ is odd} \end{cases} \tag{2-17}$$

Then the digital cross-ambiguity function (DCAF) is given by the cross-correlation function between the vectors $s^x(v)$ and w as

$$A_d^w[k,x,v] = \sum_{n=1}^{M} s_{n-k}^x(v) w_n^* \tag{2-18}$$

where $-(M-1) \leq k \leq M-1$, and $s_{n-k}^x(v)$ must be identically zero for $n-k < 1$ and $n-k > M$.
Next, consider the DCAF for integer delay k. As follows from (2-18), it is given by

$$A_d^w[k,v] = A_d^w[k,x,v]\Big|_{x=0} \tag{2-19}$$

where $A_d^w[0,0]$ is the main peak value of the DCAF. Defining the M -by-$(2M-1)$ matrix

$$S(v) = \begin{bmatrix} s_M^0(v) & \cdots & s_2^0(v) & s_1^0(v) & 0 & \cdots & 0 \\ 0 & s_M^0(v) & \cdots & s_2^0(v) & s_1^0(v) & \ddots & 0 \\ \vdots & \ddots & \ddots & \vdots & \ddots & \ddots & \vdots \\ 0 & \cdots & 0 & s_M^0(v) & \cdots & s_2^0(v) & s_1^0(v) \end{bmatrix} \tag{2-20}$$

permits to rewrite (2-18) in the matrix form as

$$r(v) = w^{\sim} S(v) \tag{2-21}$$

where the row vector $r(v) = [r_1(v), \cdots, r_{M-1}(v), r_M(v),\; r_{M+1}(v), \cdots, r_{2M-1}(v)]$ represents the DCAF (2-19) according to the relation

$$r_n(v) = A_d^w[n-M,v],\;\; n = 1,2,\ldots,2M-1 \tag{2-22}$$

and the symbol "~" denotes a hermitian or conjugate transpose. From (2-19) and (2-22), one can observe that $r_M(0)$ corresponds to the peak value of the DCAF at the point $\tau = 0, v = 0$.

2.4 Optimum weighting functions

Following (Harris, 1978; Nuttal, 1981; Van Trees, 2002) one can choose among several different approaches to the design of optimum weighting functions. In view of our intention

to minimize sidelobe level and preserve as much as possible the ridge-like behaviour of the mismatched filter response we shall follow an approach based on the physical meaning of the optimal discrete prolate sequences. For instance, in (Donald & James, 1970; Greene, 2007) the optimal discrete prolate sequence is interpreted as such a sequence that maximizes the proportion of its total power in a specified frequency interval or, referring to (Van Trees, 2002), as a weighting function that maximizes the percentage of the total power (radiated by an antenna) that is concentrated in a given angular region.

By analogy, the problem in question can be formulated as a problem of finding such a weighting function (mismatched filter) that will maximize the percentage of the total power that is concentrated in the specified mainlobe region of the DCAF. This percentage can be written as

$$\xi = \frac{\sum_{n \in R_k} \sum_{|\nu_k| \le \nu_{\max}} |r_n(\nu_k)|^2}{\sum_{n=1}^{2M-1} \sum_{|\nu_k| \le \nu_{\max}} |r_n(\nu_k)|^2}. \tag{2-23}$$

The numerator in (2-23) represents the power for a specified mainlobe region (Fig. 2-4), which is simply a sum of the squared samples of the DCAF $|r_n(\nu_k)|^2$, which belong to the set R_k that contains the points associated with the ridge for k th Doppler cut specified by the frequency $|\nu_k| \le \nu_{\max}$, where $k = 1,2,...,K = 2L+1$, $L = \nu_{\max}/\Delta\nu$, $\Delta\nu$ is the step in Doppler frequency and $\nu_{\max}$ is the maximum Doppler shift of interest. The denominator represents the full power, which is the total sum of the squared samples of the DCAF taken over all points in range (n = 1, 2,..., $2M-1$) for each Doppler cut.

The integer parameter d_k represents the shift of the peak value of the DCAF for k th Doppler cut with respect to the point τ = 0, ν = 0 (this is the point $n = M$, ν_{L+1} = 0 in Fig. 2- 4). To preserve the skew of the ridge it is reasonable to select the values of d_k to be equal to those of corresponding Doppler cuts from the digital LFM ambiguity function. The parameter m is a positive integer value that determines the width of the mainlobe region. For example, setting $m=g$ (if the oversampling factor g is a positive integer) means that the mainlobe extent is equal to that of the standard sinc-function (at the first zero points $\tau = \pm 1/B$) that correspons to a signal having rectangular spectrum of width B or to that of a zero-Doppler cut of the LFM ambiguity function $\chi(\tau, 0)$ as can be seen from (2-2) provided $BT >> 1$. In general, the value of m can be varied depending on the Doppler cut. To formally specify the mainlobe region for kth Doppler cut of the DCAF we shall use a weighting vector V_{ML}^k of the length $2M$-1. As can be seen from Fig. 2-5, for a zero-Doppler cut this vector can be written as

$$V_{ML}^{L+1} = [\underbrace{0\,0\cdots\,0}_{\substack{M-m-1 \text{ zeros} \\ \text{Sidelobe region}}}\ \underbrace{1\,\cdots\,1\,1\,1\,\cdots\,1}_{\substack{2m+1 \text{ units} \\ \text{Mainlobe region}}}\ \underbrace{0\,\cdots\,0\,0}_{\substack{M-m-1 \text{ zeros} \\ \text{Sidelobe region}}}]^{\mathrm{T}}. \tag{2-24}$$

For arbitrary k th Doppler cut this vector is given by

$$V_{ML}^{k} = [\underbrace{0\,0\cdots\,0}_{\substack{M-d_k-m-1 \text{ zeros} \\ \text{Sidelobe region}}}\ \underbrace{1\,\cdots\,1\,1\,1\,\cdots\,1}_{\substack{2m+1 \text{ units} \\ \text{Mainlobe region}}}\ \underbrace{0\,\cdots\,0\,0}_{\substack{M+d_k-m-1 \text{ zeros} \\ \text{Sidelobe region}}}]^{\mathrm{T}}. \tag{2-25}$$

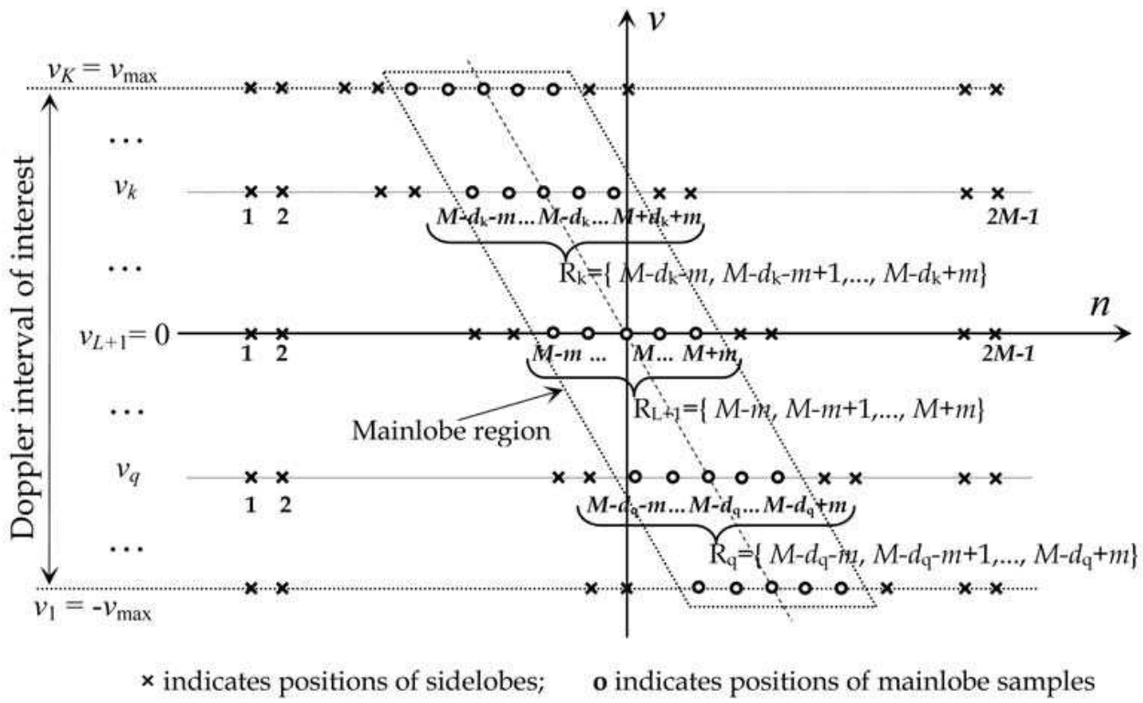

Fig. 2-4. Illustration of mainlobe region in the time-frequncy plane

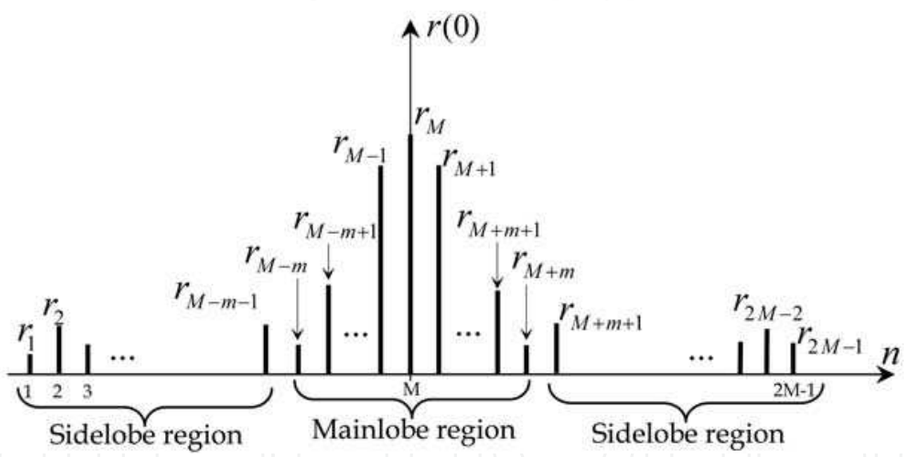

Fig. 2-5. Mainlobe and sidelobe regions for zero-Doppler cut

By using (2-25) the mainlobe power for the k th Doppler cut, which is a sum of $|r_n(v_k)|^2$ for $n \in R_k = \{M - d_k - m,\ M - d_k - m + 1,...,\ M - d_k + m\}$, can be written as

$$P_{ML}^k = \sum_{n \in R_k} |r_n(v_k)|^2 = r(v_k) Q_{ML}^k r^{\sim}(v_k) \tag{2-26}$$

where the matrix Q_{ML}^k is $(2M-1)$-by-$(2M-1)$ diagonal matrix: its diagonal is equal to the weighting vector V_{ML}^k and non-diagonal elements are zeros.
Substituting (2-21) into (2-26) yields the following real-valued quadratic form

$$P_{ML}^k = w^{\sim} B_{ML}^k w \tag{2-27}$$

where the M -by-M matrix B_{ML}^k is given by

$$B_{ML}^k = S(v_k) Q_{ML}^k S^{\sim}(v_k). \tag{2-28}$$

The total power in the mainlobe region is

$$P_{ML} = \sum_{k=1}^{K} P_{ML}^k = \sum_{k=1}^{K} w^{\sim} B_{ML}^k w = w^{\sim} B_{ML} w, \tag{2-29}$$

where the M -by-M matrix B_{ML} is given by

$$B_{ML} = \sum_{k=1}^{K} B_{ML}^k = \sum_{k=1}^{K} S(v_k) Q_{ML}^k S^{\sim}(v_k). \tag{2-30}$$

The total power in the k th Doppler cut is

$$P_{TL}^k = \sum_{n=1}^{2M-1} |r_n(v_k)|^2 = r(v_k) Q_{TL} r^{\sim}(v_k). \tag{2-31}$$

The matrix Q_{TL} in (2-31) is a $(2M-1)$-by-$(2M-1)$ unity matrix since (2-31) will present the total power only when the diagonal of Q_{TL} is equal to the weighting vector V_{TL} with all elements that are unity

$$V_{TL} = [\overset{1}{1}\ \overset{2}{1}\ \overset{3}{1}\ \cdots\ \overset{2M-2}{1}\ \overset{2M-1}{1}]^{\mathrm{T}}. \tag{2-32}$$

Using (2-21) and (2-31) yields the total power for all Doppler cuts

$$P_{TL} = \sum_{k=1}^{K} P_{TL}^k = w^{\sim} B_{TL} w \tag{2-33}$$

where the M -by-M matrix B_{TL} is given by

$$B_{TL} = \sum_{k=1}^{K} B_{TL}^k = \sum_{k=1}^{K} S(v_k) Q_{TL} S^{\sim}(v_k). \tag{2-34}$$

Thus, the ratio (2-23), which is to be maximized with respect to w, can be written as

$$\xi = \frac{w^{\sim} B_{ML} w}{w^{\sim} B_{TL} w}. \tag{2-35}$$

The maximization of the ratio (2-35) is equivalent to the following minimization problem

$$\min_{w} w^{\sim} B_{TL} w \quad \text{subject to} \quad w^{\sim} B_{ML} w = 1. \tag{2-36}$$

The solution to (2-36) can be found by minimizing the function

$$f(w, \mu) = w^{\sim} B_{TL} w + \mu (1 - w^{\sim} B_{ML} w), \tag{2-37}$$

where μ is the Langrange multiplier. Taking the gradient of (2-37) with respect to w and equating it to zero, we find that the solution to (2-36) is given by the following generalized eigenvalue problem

$$B_{TL} w = \mu B_{ML} w, \tag{2-38}$$

where μ can be interpreted as a corresponding generalized eigenvalue. It should be noted that all generalized eigenvalue in (2-38) are positive real numbers. Indeed, multiplying both sides of (2-38) by $w^{\sim}$ yields $w^{\sim} B_{TL} w = \mu w^{\sim} B_{ML} w$. As follows from (2-26)-(2-29) and (2- 31)-(2-33) $P_{TL} > 0$ and $P_{ML} > 0$ because either of the sums in (2-29) and (2-33) contains at least one real positive term $| r_M(0)|^2$, hence, the matrices B_{TL} and B_{ML} are positive definite. This proves that μ is always real positive value.

Therefore, the solution to (2-37) is the generalized eigenvector corresponding to the minimum generalized eigenvalue of (2-38). Multiplying (2-38) by B_{TL}^{-1} yields

$$B_{TL}^{-1} B_{ML} w = \frac{1}{\mu} w = \zeta w. \tag{2-39}$$

Since μ is always real and positive the minimum generalized eigenvalue $\mu_{\min}$ in (2-38) corresponds to the maximum eigenvalue $\zeta_{\max} = 1/\mu_{\min}$ in (2-39). By using this fact, the optimum weighting function (weighting coefficients of the optimum mismatched filter) can be represented as

$$w_{opt} = \mathbf{P}\left\{B_{TL}^{-1} B_{ML}\right\} \tag{2-40}$$

where $\mathbf{P}\{A\}$ is the operator, which returns the principal eigenvector of a matrix A, that is, the eigenvector corresponding to its maximum eigenvalue. As follows from (2-36), the optimum vector w_{opt} has to be normalized to satisfy the constraint in (2-36). Since any eigenvector can be normalized arbitrarily, is is clear that multiplying w_{opt} by an appropriate non-zero constant gives a vector w'_{opt}, which meets the requirement $(w'_{opt})^{\sim} B_{ML} w'_{opt} = 1$. On the other hand, it is clear from (2-35) that multiplying w_{opt} by any non-zero constant does not affect the ratio (2-35). Therefore, such normalization of w_{opt} is unimportant. In this chapter we use the vector of signal $u^x(s^x)$ and the weighting vectors w (both for the optimum and conventional weighting functions) that are normalized to be of unit norm vectors, that is, $\|u^x\| = \|s^x\| = 1$ and $\|w\| = 1$.

2.5 Numerical examples

In all numerical examples of this section, we assume an LFM signal of B = 20MHz, T = 1 μs, and the oversampling factor g = 2. Hence, N = 40 complex samples (vector of length N) are used to present the complex envelope of the LFM signal. The step in the normalized Doppler frequency $\Delta v/B$=0.005 is chosen in all calculations.

In our first example we consider the optimum weighting function of length $M = N = 40$ computed by using (2-40) with the parameter $m = g = 2$ for $v_{\max} / B$ =0, 0.05, 0.1, 0.2 and 0.4. The condition $m = g$ means that the mainlobe width of the DCAF is specified to be equal to that of a zero-Doppler cut of the LFM ambiguity function (2-2) measured at the first zeros. Table 2-1 compares the percentage of the mainlobe power (2-35) for the optimum weighting function (OF) with that for the matched filter (MF) and Kaiser window (KW). The parameter

β (Table 2-1) for the Kaiser window (in the time domain) is selected to provide the same mainlobe width as that for the optimum weighting function. The maximum sidelobe level, the loss L_w^0 in the signal-to-noise ratio (SNR) and 3 dB mainlobe broadening (all these parameters are measured in a zero-Doppler cut) for the optimum filter and Kaiser window are also included in Table 2-1.
One can easily show that the SNR loss due to weigthing is given by

$$L_w^x = \frac{|\tilde{w} s^x|^2}{\tilde{w} w \cdot s^{x\sim} s^x}, \quad 0 < L_w^x \le 1. \tag{2-41}$$

The 3dB mainlobe broadening is defined as the ratio $b_{ML} = W_{WF}/W_{MF}$ where W_{WF} and W_{MF} are the mainlobe width at –3 dB level for a zero-Doppler cut of the DCAF in case of mismatched filtering (for conventional or optimum weighting functions) and digital LFM ambiguity function (matched filtering), respectively.

$\frac{v_{max}}{B}$	Percentage of the mainlobe power ξ, %			Maximum sidelobe, dB		SNR loss L_w^0, dB/ β		3dB mainlobe broadening, b_{ML}	
	MF	KW	OF	KW	OF	KW	OF	KW	OF
0	90.979	97.201	99.541	-20.6	-29.2	-0.483/2.7	-0.772	1.21	1.21
0.05	90.997	97.060	99.531	-20.2	-29.1	-0.442/2.6	-0.769	1.20	1.20
0.1	91.047	96.901	99.502	-19.8	-29.1	-0.402/2.5	-0.761	1.19	1.19
0.2	91.229	96.716	99.393	-19.5	-28.8	-0.363/2.4	-0.767	1.17	1.17
0.4	91.282	96.330	99.157	-18.7	-28.8	-0.289/2.2	-0.805	1.16	1.16

Table 2-1. Comparison of the matched filter (MF), Kaiser weighting (KW) and optimum filter (OF) in terms of the mainlobe power percentage, maximum sidelobe, SNR loss and mainlobe broadening for the optimum filter of length M= N = 40 designed for m = g=2

As can be seen from Table 2-1, the percentage of the mainlobe power (ξ) for the optimum weigthing exceeds those for the matched filter and Kaiser window by about 8.5% and 2.5%, respectively, for a wide range of the Doppler interval of interest ($|v_{max}|/B \le 0.4$). Despite these relatively small gains in ξ the optimum weigthing provides appreciable reduction in sidelobes. As one can see, the maximum sidelobe level measured in a zero- Doppler cut is about –29 dB; this is by 15 dB below that for the matched filter and by about 9 dB below that for the KW (under the conditions the data in Table 2-1 are computed). The price paid for the sidelobe suppression is quite low. Indeed, the SNR loss for the OF is about -0.8 dB with respect to that of the MF and –(0.3 … 0.5) dB as compared to that for the KW. Second, the mainlobe broadening against the MF is also relatively small, it ranges from 1.21 to 1.16 for $|v_{max}|/B$ = 0, 0.05, 0.1, 0.2 and 0.4, respectively.
Fig. 2-6 illustrates the sidelobe suppression for the optimum weighting by comparing a zero-Doppler cut of the digital cross-ambiguity function for the optimum filter (designed for v_{max}/B = 0.1) with corresponding zero-Doppler cuts for the Kaiser window and matched filter. To get more pictorial view for comparison all these cuts are normalized so that the magnitudes of their peak values are equal to unity (zero on the dB-scale). The Doppler tolerance of the optimum filter is illustrated in Fig. 2-7 that compares the ridge (peak signal amplitude) of the DCAF for the optimum filter (v_{max}/B = 0.1) with those for the

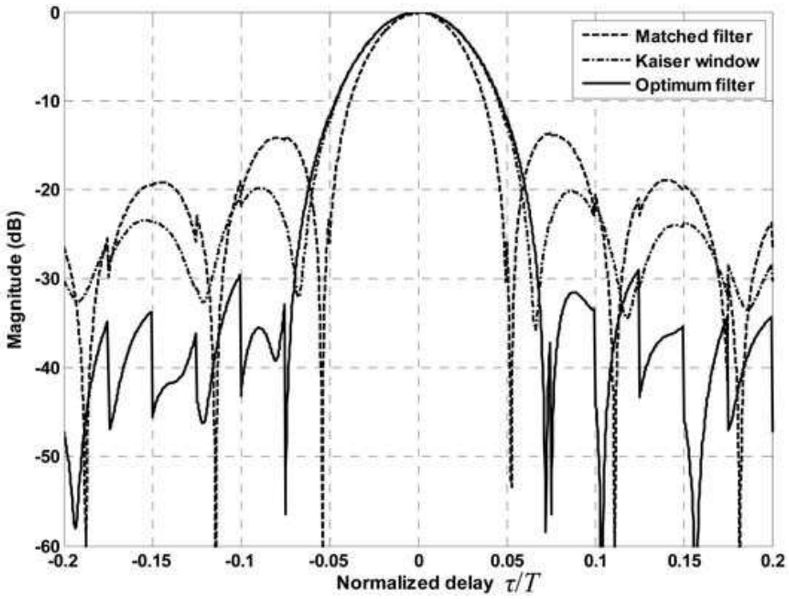

Fig. 2-6. Zero-Doppler cuts of digital cross-ambiguity functions for the optimum filter (M=N=40, m=g=2, $v_{\max}/B$ = 0.1) and Kaiser window and zero-Doppler cut of digital ambiguity function for the matched filter

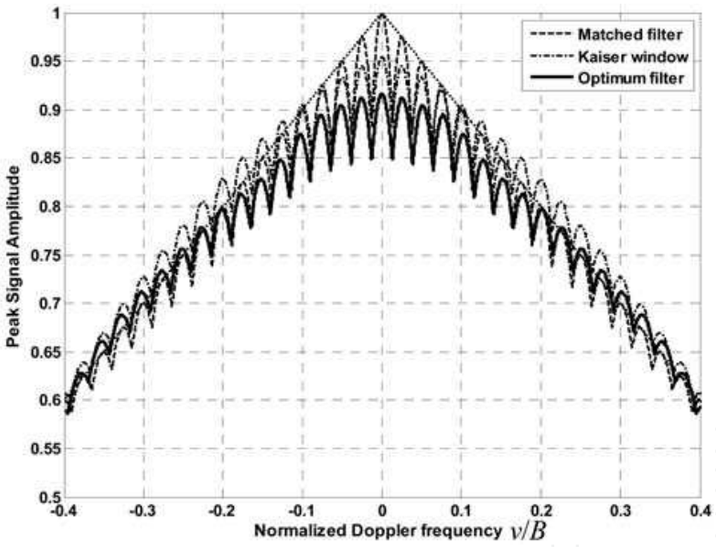

Fig. 2-7. Doppler tolerance of the optimum filter designed with M=N=40 and m=g=2 for $v_{\max}/B$ = 0.1

corresponding Kaiser window and matched filter. As one can see in Fig. 2-7, for $|v|/B \le 0.1$ the ridge of the DCAF for the optimal filter goes slightly below that for the Kaiser window (due to the SNR loss of – 0.36 dB). This means that the optimum filter maximizes the ratio (2-35) chiefly through the sidelobe suppression.

In the second example we illustrate a new feature of the proposed optimum weighting that convetional weightings do not possess in principle. This feature can be realized when the parameter m, which determines the width of the mainlobe region in time delay, is less than

the oversampling factor *g*. The condition $m<g$ means that the mainlobe width of the DCAF is specified to be less than that for a zero-Doppler cut of (2-2) measured at the first zeros. Since the optimum filter is designed under this condition the maximum percentage of the mainlobe power is concentrated within a narrower "strip" than for the matched filter. Hence, one should expect that there will be no mainlobe broadening and no range resolution degradation with respect to the matched filter.

Table 2-2 presents the percentage of the mainlobe power, maximum sidelobe level, the SNR loss L_w^0 and 3dB mainlobe broadening (in zero-Doppler cut) for the OF of length M=1.2N=48 designed under the condition $m = g - 1 = 1$. Since there is no simple formula that directly relates the SNR loss L_w^x to m and M for the OF, it was numerically found for $N \le M \le 1.5N$ that the SNR loss does not exceed 3 dB and the maximum sidelobe level is approximately minimized at M= 1.2N= 48 for all v_{max}/B given in Table 2-2.

$\frac{v_{max}}{B}$	Percentage of the mainlobe power ξ, % OF / MF	Maximum sidelobe, dB	SNR loss, dB	3dB mainlobe broadening, b_{ML}
0	99.351 / 90.730	-22.1	-1.426	0.97
0.05	99.302 / 90.651	-22.3	-1.459	0.96
0.1	99.172/ 90.429	-22.8	-1.571	0.95
0.2	98.725 / 89.556	-23.6	-2.120	0.92
0.4	98.275 / 88.631	-20.3	-2.775	0.89

Table 2-2. Percentage of the mainlobe power for optimum filter/matched filter (OF/MF), maximum sidelobe, SNR loss and mainlobe broadening for optimum filter of length M= 1.2N = 48 designed for $m = g$-1=1 at different v_{max}/B

As can be seen from Table 2-2, for the optimum weighting with M = 48, m = 1 the 3dB mainlobe broadening b_{ML} <1, as expected. Therefore, there is no degradation in the range resolution with respect to the matched filter. The price paid for this is relatively large SNR loss (from –1.5dB to –2.8dB depending on the Doppler extent v_{max}/B) and an increase in the maximum sidelobes (about 8 dB) with respect to the OF designed under the condition $m=g$ (see Table 2-1). At the same time the maximum sidelobe level is somewhat lower (by about 1.5 dB) than that for the Kaiser window from Table 2-1.

The behaviour of the DCAF for the OF designed with M =48, m=1 for v_{max}/B=0.1 is illustrated by Figs. 2-8 – 2.10. Fig. 2-8 compares a zero-Doppler cut of the DCAF for the OF with that for the matched filter. The Doppler tolerance of this filter is illustrated in Fig. 2-9. The digital cross-ambigutiy functions (3-D presentations) and corresponding contour plots (at two levels of -3.92dB and -13.32dB) for the optimum filters with M = 40, m = 2 and M = 48, m = 1 (both are designed for v_{max}/B=0.1) are shown in Fig. 2-10 (a) and (b), respectively.

Analyzing the plots in Fig. 2-8 and Fig. 2-9 and the percentage of the mainlobe power for the OF and MF (Table 2-2) we again arrive at the conclusion that the optimum filter (2-40) chiefly maximizes the ratio (2-35) by supressing the sidelobes. Comparing Fig 2-10 (a) and (b) reveals increased sidelobes: additional contour lines at a level of -13.32 dB in the latter. This increase in sidelobe level is due to narrower mainlobe region for the OF with M =48, m =1 against that for the OF with M =40, m =2. The fundamental property of the cross-ambiguty function says that it is impossible to remove energy from one portion of the cross-ambiguity surface without placing it somewhere else on the (τ, v) plane.

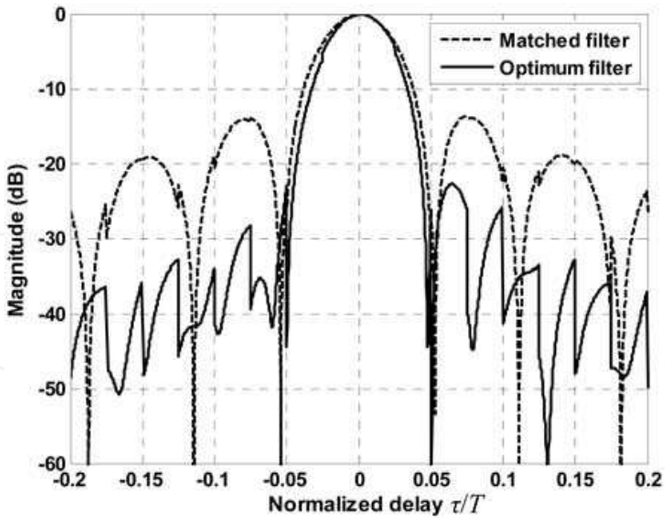

Fig. 2-8. Zero-Doppler cuts for the optimum (M= 48, m= 1) and matched filters

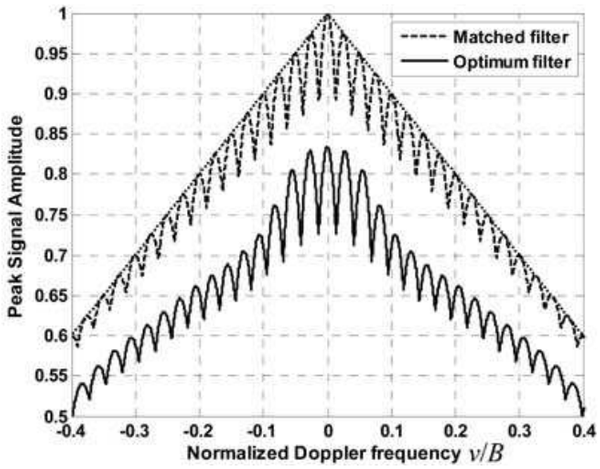

Fig. 2-9. Doppler tolerance of the optimum filter with M= 48, m= 1 ($\nu_{\max}/B$ = 0.1)

3. Optimization of InSAR accuracy performance

This section addresses the improvement of the interferometric synthetic aperture radar (InSAR) performance, namely, minimization of the standard deviation of the height estimate through the optimization of the weighting coefficients of a digital filter to be used in the InSAR receiving channels for pulse compression in range and in azimuth dimension. For simplicity we consider only the pulse compression in range.

The matched filter is an optimum filter under the criterion of maximum signal-to-noise ratio (SNR) in the presence of white noise. This section deals with such a filter that approximates to an optimum filter under a different criterion: the minimum of the height-standard deviation σ_h. As is well known, (e.g., Rosen et al., 2000) applying conventional weighting in the InSAR receiving channels allows decreasing σ_h against matched filtering although the SNR in the event of weighting is inevitably less than that in the event of matched filtering. Thus, strictly speaking, the optimum filter in terms of the minimum of the height-standard deviation σ_h belongs to a class of mismatched filters.

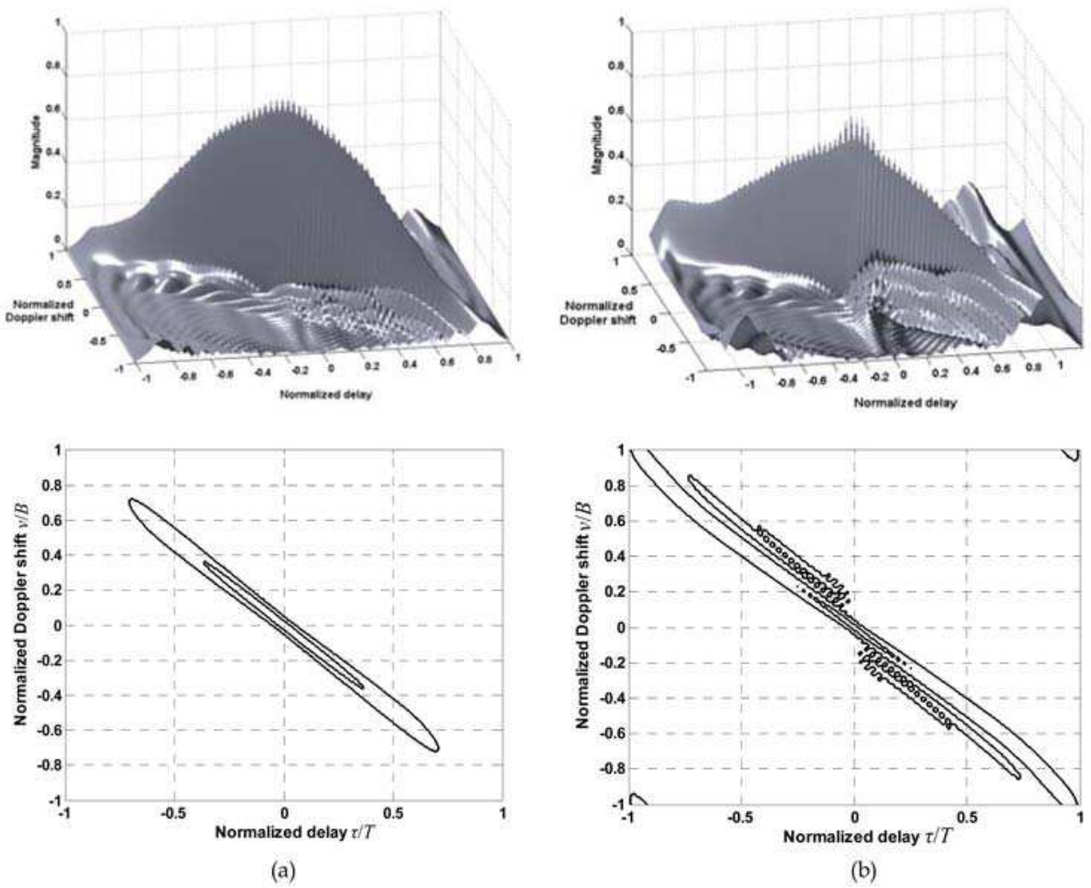

Fig. 2-10. Digital cross-ambiguity functions and corresponding contour plots (below) for optimum filters with (a) M= 40, m= 2 and (b) M= 48, m= 1 ($v_{\max}/B$ = 0.1)

3.1 Height estimation accuracy

The magnitude γ of the full correlation function between InSAR channels is given by $\gamma = \gamma_G \gamma_N \gamma_Z \gamma_T$ (Rosen et al., 2000), where γ_G is the geometric (baseline) correlation, γ_N is the correlation due to thermal noise in the interferometric channels, γ_Z is the correlation due to volume scattering, and γ_T represents the temporal correlation (in repeat-pass systems). From (Rodriguez & Martin, 1992; Rosen et al., 2000) it follows that increasing γ results in decreasing the standard deviation of inferred interferometric phase estimates and correspondingly derived height values.

As has been pointed out in (Baskakov&Ka, 2000; Rosen et al., 2000), modifying the system point target response (PTR) in range by applying different weighting functions in the InSAR receiving channels, one can change the shape of the geometric correlation γ_G to reduce the phase noise. It should be noted, that as has been shown (Gatteli et al., 1994) one can obtain γ_G = 1 (at least theoretically) by using a kind of band-pass filtering (Rosen et al., 2000) of signals from both channels so that they have slightly different center frequencies. The relationship between these frequencies depends on the look angle and surface slope, so that an adaptive iterative procedure is needed to implement this approach (Rosen et al., 2000). In this paper we will try deriving benefits from practically much simpler approach, which is based on using weighting.

The major implication of weighting in an InSAR is that it allows increasing the total correlation γ due to increasing the geometric correlation γ_G, and, consequently, reducing height estimation errors, other conditions being equal. Examples given in (Rosen, et al., 2000) for conventional weighting functions demonstrate improved shapes of geometric correlation with weightings against that for a standard sinc response with no weighting.

However, at least two significant problems associated with weighting have not been discussed in (Rosen et al., 2000). First, it is well-known, that applying weighting inevitably leads to the signal-to-noise (SNR) degradation in the interferometric channels, which, in turn, results in decreasing the correlation due to thermal noise γ_N. If this decrease in γ_N prevails over an increase in γ_G, then the full correlation γ will degrade that finally results in deterioration of the height estimation accuracy. Another problem associated with weighting is degradation of the InSAR resolution due to mainlobe broadening of the PTR in range.

The effect of conventional weighting on the InSAR performance was analyzed in (Baskakov & Ka, 2000) for Hamming and Gauss weightings. It has been claimed that conventional weighting gives an improvement in the height accuracy only for small relative baselines [the ratios of B(see Fig. 3-1) to the wavelength λ], while for large relative baselines weighting leads to significant deterioration in performance.

The maximum-likelihood (ML) estimator presented in (Rodriguez & Martin, 1992) can be used as an accurate estimator of the interferometric phase from homogeneous distributed targets. That ML estimator is unbiased modulo 2π, and its standard deviation can be easily obtained by using Monte-Carlo simulations. The Cramér-Rao lower bound (CRLB) on the standard deviation σ_Φ in unbiased estimation of the interferometric phase is given by

$$\sigma_\Phi = \frac{1}{\sqrt{(2N_L)}} \frac{\sqrt{1-\gamma^2}}{\gamma} \tag{3-1}$$

where N_L is the number of looks. It has been shown (Rodriguez & Martin, 1992) that the phase-standard deviation of the ML estimator approaches the limit given by (3-1) very rapidly with number of looks for the first four looks, especially if the correlation γ is high. Hence, formula (3-1) gives a reasonable approximation for the phase-standard deviation of the ML estimator when the inequality $N_L \geq 4$ holds true.

Using (3-1) one can relate the full correlation to height estimation errors as (Rodriguez & Martin, 1992; Ka & Kononov 2007)

$$\sigma_h = \frac{\lambda H \tan\theta}{2\pi B_n} \frac{1}{\sqrt{(2N_L)}} \frac{\sqrt{1-\gamma^2}}{\gamma} \tag{3-2}$$

where σ_h is the standard deviation of height errors, H is the height of a spacecraft, $B_n = B \cos(\alpha - \theta)$ is the projection of the baseline B (in section 2 B denoted the LFM signal bandwidth) onto the direction perpendicular to the look direction, and α and θ are the baseline tilt and look angles, respectively (Fig. 3-1). As was shown (Rodriguez & Martin, 1992) , σ_Φ is minimized, hence, σ_h is also minimized, by choosing $\alpha = \theta$.

In what follows we assume that the system operates in standard mode of data collection (Rosen et al., 2000) and its two interferometric channels have identical PTRs of the separable form $\chi_r(\rho) \cdot \chi_a(s)$, where $\chi_r(\rho)$ and $\chi_a(s)$ are the system PTR in range (ρ) and azimuth (s), respectively. For simplicity, we confine our analysis to the range dimension although the proposed technique can be also used in the azimuth dimension. To reveal the potential of

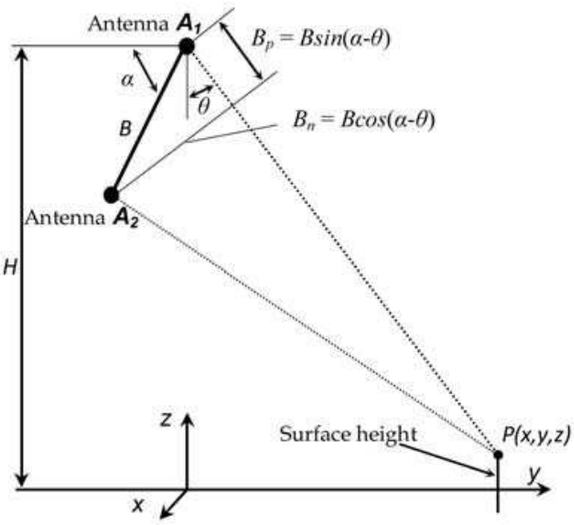

Fig. 3-1. Interferometric SAR looking geometry

the proposed technique we assume that the surface slope and coregistration errors can be neglected and the interferometric channels have equal center frequencies. Then, one can show that the general equation for γ_G (Rosen et al., 2000) reduces to

$$\gamma_G(\kappa_\rho) = \frac{\left| \int \left| \chi_r(\rho) \right|^2 \exp\left[-j\kappa_\rho \rho \right] d\rho \right|}{\int \left| \chi_r(\rho) \right|^2 d\rho} \tag{3-3}$$

where $\kappa_\rho = \kappa B_n / (r_o \tan\theta)$ is the interferometric fringe wavenumber in range ($\kappa = 2\pi/\lambda$ is the wavenumber) and r_o = H/cosθ is the slant range from the system to the middle point of a distributed resolution cell at the centre of the swath.

When the PTR in range is given by a standard sinc-function $\chi_r(\rho) = \sin(\pi\rho/R)/(\pi\rho/R)$, where $R = c/(2F_m)$ is the intrinsic range resolution (c is the speed of light and F_m is the system bandwidth), the geometric correlation was shown (Rodriguez & Martin, 1992; Ka & Kononov, 2007) to be given by

$$\gamma_G = 1 - \frac{R}{r_o \tan\theta} \frac{B_n}{\lambda}. \tag{3-4}$$

The second term γ_N is the correlation due to thermal noise alone. As was shown in (Rodriguez & Martin, 1992), assuming isotropic backscatter coefficient within the SAR resolution element, γ_N can be represented as

$$\gamma_N = \frac{1}{1+q^{-1}} \tag{3-5}$$

where q is the system signal-to-noise ratio (SNR), which is assumed to be equal in both channels.

The correlation term γ_Z is given by (Rodriguez & Martin, 1992; Ka & Kononov, 2007)

$$\gamma_Z = \exp\left[-2\pi^2 \left(\frac{\sigma_s}{H \tan\theta} \frac{B_n}{\lambda} \right)^2 \right] \tag{3-6}$$

where σ_s is the height standard deviation of specular points with respect to the mean topography.
The term γ_T is specific to repeat-pass systems (Rosen et al., 2000; Zebker & Villasenor, 1992) and represents a measure of decorrelation between two images (forming an interferogram) due to change in the surface itself over the temporal interval between the times when the images are acquired. In what follows we assume $\gamma_T = 1$.

3.2 Optimization of PTR

Examining (3-3) yields that its right-hand side has the form of a Fourier transform. From the Fourier transform properties, it follows that the narrower the PTR $\chi_r(\rho)$ in time (range) domain, the wider the baseline correlation function γ_G (3-3) and the better InSAR height estimation performance, other conditions being equal. For a given transmit signal, one of the possible ways to concentrate the PTR in range domain is designing such a receiving filter, which maximizes the percentage of the total power within a specified time interval around the PTR peak value point. To control the range resolution the length of this interval (mainlobe region) can be adjusted.
Noting that the module of PTR in range is a zero-Doppler cut (in case of ideal frequency stability of radar transmitter) of the cross-ambiguity function allows concluding that the method of section 2 can be directly used to optimize the PTR for the purpose of improving the accuracy of InSAR height measurements.
Then, as follows from equation (2-21), the digital PTR can be written as

$$r = r(0) = w^{\sim} S(0) \tag{3-7}$$

where the row vector $r = [r_1(0), \cdots, r_{M-1}(0), r_M(0), r_{M+1}(0), \cdots, r_{2M-1}(0)]$ represents the digital PTR $\chi_{dr}[\cdot]$, i.e., a zero-Doppler cut of the DCAF, according to the relation

$$r_n = r_n(0) = A_d^w[n-M, 0] = \chi_{dr}[n-M], \;\; n = 1, 2, ..., 2M-1 \tag{3-8}$$

Next, as can be seen from (2-23), for the problem in question the ratio to be maximized is

$$\xi = \frac{\sum\limits_{n \in R_{L+1}} |\chi_{dr}[n-M]|^2}{\sum\limits_{n=1}^{2M-1} |\chi_{dr}[n-M]|^2} = \frac{\sum\limits_{n=M-m}^{M+m} |r_n|^2}{\sum\limits_{n=1}^{2M-1} |r_n|^2} \tag{3-9}$$

where the set $R_{L+1} = \{ M-m, ..., M-1, M, M+1, ..., M+m \}$ represents the specified mainlobe region around the PTR peak point.
Based on the derivation in section 2.4 one can write the solution for the optimum weighting function that maximally concentrates the PTR in range in terms of the ratio (3-9) as

$$w_{opt} = \mathbf{P}\{B_{TL}^{-1} B_{ML}\}. \tag{3-10}$$

The matrices B_{TL} and B_{ML} in (3-10) are given by

$$B_{TL} = SQ_{TL}S^{\sim} \text{ and } B_{ML} = SQ_{ML}S^{\sim} \tag{3-11}$$

respectively, where S=S(0) [see formula (2-20)] and the matrix Q_{ML} is (2M −1)-by- (2M −1) diagonal matrix: its diagonal is equal to the weighting vector V_{ML}^{L+1} [see (2-24)] and non-diagonal elements are zeros.

3.3 Numerical examples

Numerical examples illustrate the InSAR height accuracy and range resolution that can be achieved by using the optimum weighting function (3-10) for an LFM signal with T = 3 μs and B = 20 MHz. The oversampling factor g = 2 was chosen. Hence, the complex envelope of the LFM signal is given by a vector of length N = 120. To compute the baseline correlation function for digital interferometric channels the following digital counterpart of equation (3-3) was used

$$\gamma_G = \frac{\left|\sum_{i=-M+1}^{M-1} |\chi_{dr}[i,x]|^2 \exp\left[-j\kappa_\rho (i\cdot\Delta R_s)\right]\right|}{\sum_{i=-M+1}^{M-1} |\chi_{dr}[i,x]|^2}, \quad \Delta R_s = cT_s/2. \tag{3-12}$$

where $\chi_{dr}[i,x] = A_d^w[i,x,0]$, see equation (2-18).

To quantify the change in the PTR mainlobe width due to weighting we use the 3dB mainlobe broadening parameter b_{ML} defined in subsection 2.5.

It can be shown, for a single SAR resolution element with isotropic backscatter coefficient, that in the event of mismatched filtering the SNR can be represented as

$$q = L_w^x q_{MF} \tag{3-13}$$

where q_{MF} is the SNR for the matched filter and L_w^x is the loss in SNR (due to weighting), which is given by equation (2-41).

Since there are no simple closed-form expressions that directly relate the coefficient of loss L_w^x to m and M for the optimum weighting filter given by (3-10), it was numerically found for m=g−1, g, g+1, i.e., for m = 1, 2, and 3 that the SNR loss is approximately minimized for 1.1N ≤ M ≤ 1.5N. The parameters L_w^0 and b_{ML} for the optimum filter of length M =132 computed from (3-10) for m = 1, 2, 3 are summarized in Table 3-1. To estimate the mainlobe width, the digital PTRs were computed by using (2-18) at integer points −(M−1) ≤ k ≤ M−1 and between them for x = 0.01, 0.02,..., 0.99 . For comparison, the SNR loss and parameter β for the Kaiser window of length M = 132 are also given. The parameter β was selected to approximately provide the same value of b_{ML}, except for m = 1 (it is impossible for the Kaiser window to find such a parameter β , at which b_{ML} < 1). As can be seen from Table 3-1, for the optimum filter of length M = 132 at m = 2 the degradation in range resolution is quite appreciable (mainlobe broadening is 20%) and the SNR loss is relatively small (about –0.7 dB). The optimum filter with M =132, m = 1 gives a quite noticeable enhancement in the range resolution with respect to the matched filter. The price paid for this is relatively large SNR loss (about –3 dB) and an increase of 10% in the filter length. It will be shown that despite the relatively large SNR loss this optimum filter provides appreciable improvement

Parameter m	Optimum filter M = 132		Kaiser window N = 132	
	L_w^0, dB	b_{ML}	L_w^0, dB	β
1	-3.08	0.96	–	–
2	-0.72	1.20	-0.43	3.1
3	-1.07	1.36	-0.97	4.8

Table 3-1. SNR loss and PTR mainlobe broadening with weighting

in height accuracy. The range resolution enhancement for the optimum filter with M =132, m = 1 is evident from Fig. 3-2 that shows the magnitude of the digital PTR for the optimum filter in comparison with those for the Kaiser window (β = 3.1) and matched filter. To get more pictorial view, all the PTR's are normalized so that the magnitudes of their peak values are equal to unity (zero on the dB-scale).

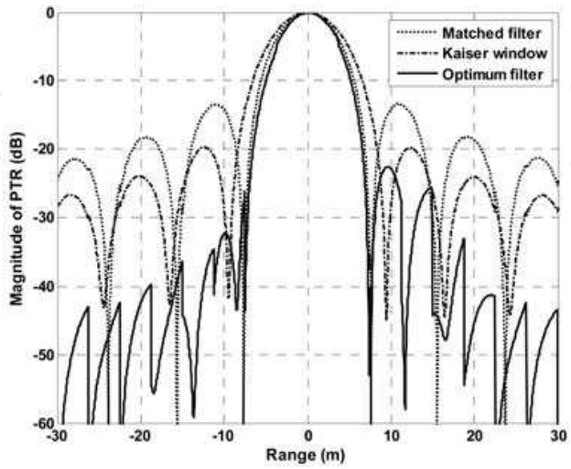

Fig. 3-2. Range resolution enhancement for the optimum filter

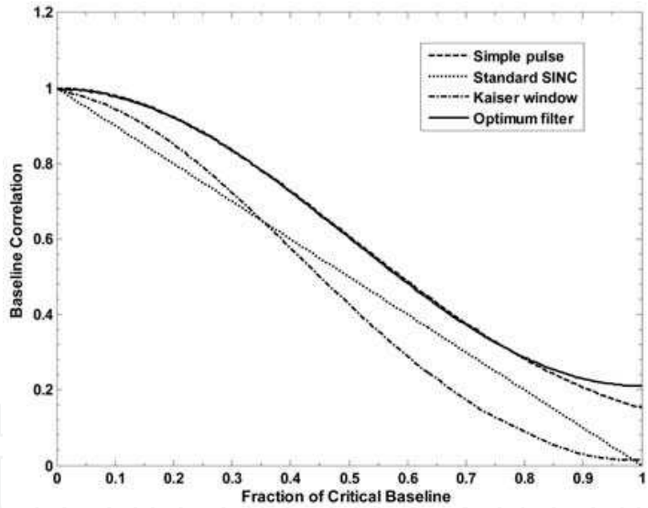

Fig. 3- 3. Baseline correlation functions for various point-target responses

Fig. 3-3 displays the baseline correlation functions corresponding to the digital PTR's for the optimal filter and Kaiser window shown in Fig. 3-2. For comparison, the baseline correlations for the standard sinc response and for the response of a filter matched to a simple rectangular pulse with pulsewidth 1/ F_m are also plotted. A remarkable feature of the PTR for the simple rectangular pulse is that it has zero sidelobes outside of the mainlobe region for m=g. Therefore, the baseline correlation function for the simple rectangular pulse can be used as an example of ideal reference model for comparison. From the inspection of Fig. 3-3, one can conclude that narrowing the mainlobe region in designing an optimum filter allows a distinct improvement in the shape of the baseline correlation function in the sense of the phase (height) noise reduction. As can be seen, the baseline correlation curve for

the optimal filter goes appreciably higher than those for the Kaiser window and standard sinc function and almost coincides with that corresponding to the simple rectangular pulse.
As mentioned above, the SNR degradation due to weighting may result in a significant decrease in the correlation due to thermal noise γ_N and, finally, in performance deterioration. Thus, to draw a final conclusion concerning the effectiveness of the suggested approach one has to evaluate a potential improvement in the InSAR accuracy performances taking into account all the components of the full correlation. In Fig. 3-4 and Fig. 3-5 we plot for the optimal filter with M = 132 and m = 1, the height standard deviation σ_h calculated by using (3-2), (3-5), (3-6), (3-12) and (3-13) with inputs x = 0 , N_L = 9, θ =α = 30°, H = 350 km, σ_s = 1 m, and γ_T = 1 versus SNR for B_n/λ = 1500 and versus the relative baseline B_n/λ for SNR=18dB, respectively. The calculations were also done at x = 0.5, which can be interpreted as a subpixel shift. The performance degradation for x = 0.5 (with respect to x = 0) did not exceed 15%. The performances for the matched filter, Kaiser window (β =3.1) and the simple pulse are also plotted (for x = 0).

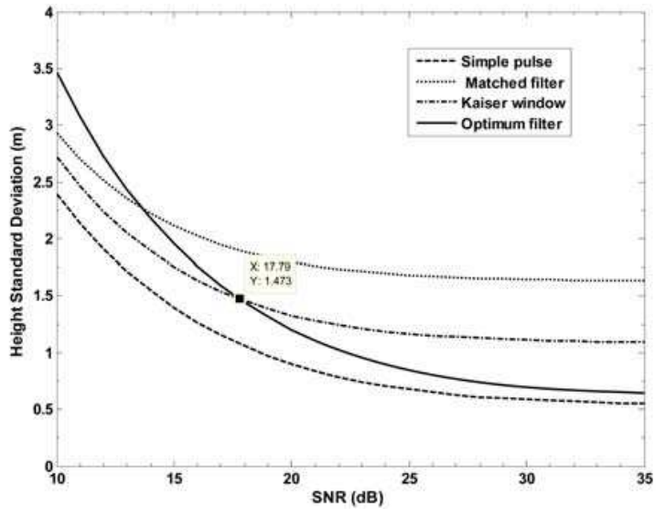

Fig. 3-4. Height-standard deviation σ_h versus signal-to-noise ratio (SNR) for B_n/λ = 1500

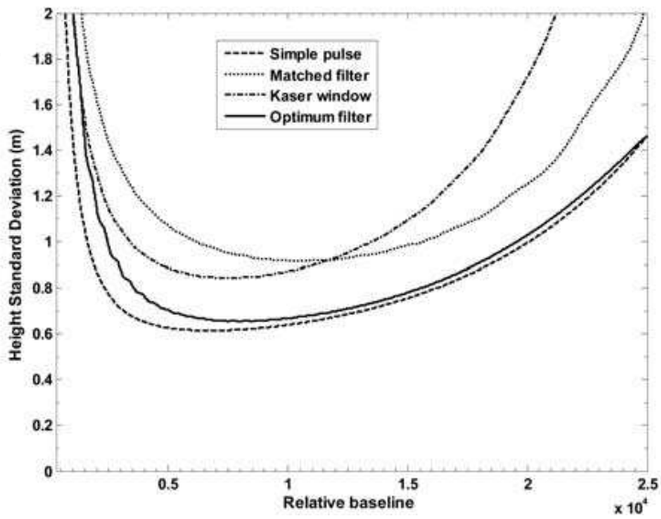

Fig. 3-5. Height-standard deviation σ_h versus relative baseline B_n/λ for SNR = 18 dB

It is clear from Fig. 3-4 that no performance improvement results for SNR<17.79 dB, but the improvement becomes noticeable when the SNR is on the order of 20 dB or larger. As can be seen from Fig. 3-5, despite the relatively large SNR loss this optimum filter provides appreciable improvement in height estimation accuracy against the matched filter and Kaiser window over a wide range of the relative baseline.

4. Conclusion

This chapter has introduced a new approach for the design of optimum weighting functions. By analogy with optimal discrete prolate sequences this approach considers the design of weighting functions as a problem of finding such a digital mismatched filter that will maximize the proportion of the total response power that is concentrated in the specified time-frequency region. A closed-form matrix equation to numerically design the optimum weigthing functions has been derived.

Two applications of the proposed approach have theoretically been addressed in the chapter. First, the problem of the optimum Doppler-tolerant pair signal-filter design when a given signal is specified to be an LFM signal and, second, the specification of weighting functions for interferometric synthetic aperture radars with the purpose of improving the accuracy of height measurements, have been considered.

There has been shown, for the first application, that the proposed optimum weighting functions (mismatched filters) provide significant sidelobe suppression with respect to conventional weighting functions at relatively low SNR loss. It has also been shown that they can provide appreciable improvement in the accuracy of height measurements, as compared to conventional weightings, for interferometric synthetic aperture radars.

A remarkable feature of the suggested optimum weightings is that improvement in the sidelobe suppression and height accuracy can be achieved without degradation in range resolution that is inevitable in the case of using traditional weighting functions.

5. References

Barton, D.K., (2005). *Radar System Analysis and Modeling*, Artech House, ISBN 1-58053-681-6, Norwood.

Baskakov, A.I. & Ka, M.-H., (2000). Analysis of the effect of phase noise on the accuracy characteristics of interferometric fixed-baseline SARs, *Earth Observations and Remote Sensing*, Vol. 16, 2000, pp. 247-256.

Blankenship, P., & Hofstetter, E., (1975). Digital Pulse Compression via Fast Convolution, *IEEE Trans. on Acoustic, Speech, and Signal Processing,* Vol. ASSP-23, No. 2, April 1975, pp. 189-201.

Cook, C. & Bernfeld, M. (1967). *Radar Signals: An Introduction to Theory and Application*, Academic Press, ISBN 0-89006-733-3, New York.

Curlander, J. & McDonough, R. (1991). *Synthetic Aperture Radar: Systems and Signal Processing*, Wiley, ISBN 0-471-85770-X, New Jersey.

Donald, T. & James, F. (1970). Designing Digital Low-Pass Filters – Comparison of Some Methods and Criteria, *IEEE Trans. on Audio and Electroacoustics*, Vol. AU-18, No. 4, December 1970, pp. 487-494.

Gatteli F. et al., (1994). The wavenumber shift in SAR interferometry, *IEEE Trans. Geoscience Remote Sensing*, Vol. 32, No. 4, July 1994, pp. 855-864.

Greene, M., (2007). The discrete prolate spheroidal sequences and a series expansion for seismic wavelets, *GEOPHYSICS*, Vol. 72, No. 6, November-December 2007, pp. V119-V132.

Harris, F. J. (1978). On the Use of Windows for Harmonic Analysis with the Discrete Fourier Transform, *Proceedings of the IEEE*, Vol. 68, No. 1, January 1978, pp. 51-83.

Ka, M.-H. & Kononov, A. (2007). Effect of look angle on the accuracy performance of fixed-baseline interferometric SAR, *IEEE Geoscience Remote Sensing Letters*, Vol. 4, No. 1, January 2007, pp. 65-69.

Levanon, N. & Mozeson, E. (2004). *Radar Signals*, Wiley, ISBN 0-471-47378-2, New Jersey.

Nuttal, A. (1981). Some windows with very good sidelobe behavior, *IEEE Trans. On Acoustics, Speech, and Signal Processing*, Vol. 29, No. 1, February 1981, pp. 84-91.

Peebles, P., JR., (1998). *Radar Principles*, Wiley, ISBN 0-471-25205-0, New York.

Richards, M. (2005). *Fundamentals of Radar Signal Processing*, McGraw-Hill, ISBN 0-07-144474-2, New York.

Rodriguez, E. & Martin, J. (1992). Theory and design of interferometric synthetic aperture radars, *Radar and Signal Processing*, *IEE Proceedings F*, Vol. 139, No. 2, April 1992, pp. 147-159, ISSN 1751-8784.

Rosen, P.A. et al., (2000). Synthetic aperture radar interferometry, *Proceedings IEEE*, Vol. 88, No. 3, March 2000, pp. 333-382.

Skolnik, M. (2008). *Radar Handbook*, 3rd ed., McGraw-Hill, ISBN 978-0-07-148547-0, New York.

Van Trees, H. L., (2002). *Detection, Estimation, and Modulation Theory, Part IV, Optimum Array Processing*, Wiley, ISBN 0-471-09390-4, New York.

Zebker H. A. & Villasenor, J., (1992). Decorrelation in interferometric radar echoes, *IEEE Trans. Geosci. Remote Sens.* Vol. 30, No. 5, September 1992, pp. 950-959.

Convergence and Hybrid Information Technologies

Edited by Marius Crisan

ISBN 978-953-307-068-1
Hard cover, 426 pages
Publisher InTech
Published online 01, March, 2010
Published in print edition March, 2010

Starting a journey on the new path of converging information technologies is the aim of the present book. Extended on 27 chapters, the book provides the reader with some leading-edge research results regarding algorithms and information models, software frameworks, multimedia, information security, communication networks, and applications. Information technologies are only at the dawn of a massive transformation and adaptation to the complex demands of the new upcoming information society. It is not possible to achieve a thorough view of the field in one book. Nonetheless, the editor hopes that the book can at least offer the first step into the convergence domain of information technologies, and the reader will find it instructive and stimulating.

InTech Europe
University Campus STeP Ri
Slavka Krautzeka 83/A
51000 Rijeka, Croatia
Phone: +385 (51) 770 447
Fax: +385 (51) 686 166
www.intechopen.com

InTech China
Unit 405, Office Block, Hotel Equatorial Shanghai
No.65, Yan An Road (West), Shanghai, 200040, China
中国上海市延安西路65号上海国际贵都大饭店办公楼405单元
Phone: +86-21-62489820
Fax: +86-21-62489821

IntechOpen